Article

The Effects of Molecular Packing Behavior of Small-Molecule Acceptors in Ternary Organic Solar Cells

Eunhee Lim

Department of Chemistry, Kyonggi University, 154-42 Gwanggyosan-ro, Yeongtong-gu, Suwon 16227, Korea; ehlim@kyonggi.ac.kr

Abstract: Herein, two diketopyrrolopyrrole (DPP)-based, small-molecule isomers, *o*- and *p*-DPP-PhCN, were introduced as acceptors in ternary organic solar cells (OSCs). The isomers have the same molecular backbone but differ in the positions of the cyanide (CN) substituents (ortho and para), which greatly affects their packing behavior. Ternary solar cells composed of poly(3-hexylthiophene) (P3HT):DPP-PhCN:phenyl-C_{61}-butyric acid methyl ester (PCBM) were fabricated, and the effects of the different packing behaviors of the third component on the device performance and the working mechanism of the ternary cells were investigated. The addition of *o*-DPP-PhCN with a relatively high-lying lowest unoccupied molecular orbital energy level resulted in an increase in the open-circuit voltage (V_{OC}) in the ternary devices, demonstrating the alloy-like structure of the two acceptors (*o*-DPP-PhCN and PCBM) in the ternary system. However, the *p*-DPP-PhCN-based ternary cells exhibited V_{OC} values similar to that of a P3HT:PCBM binary cell, irrespective of the addition of *p*-DPP-PhCN, indicating a cascade energy-level structure in the ternary system and an effective charge transfer from the P3HT to the PCBM. Importantly, by increasing the addition of *p*-DPP-PhCN, the short-circuit current density increased substantially, resulting in pronounced shoulder peaks in the external quantum efficiency responses in the long-wavelength region, corresponding to the contribution of the photocurrent generated by the light absorption of *p*-DPP-PhCN. Despite sharing the same molecular backbone, the two DPP-PhCNs exhibited substantially different packing behaviors according to the position of their CN substituents, which also greatly affected the working mechanism of the ternary devices fabricated using the DPP-PhCNs as the third component.

Keywords: organic solar cell; organic photovoltaic cells; OSC; OPV; ternary cell; diketopyrrolopyrrole; DPP; nonfullerene; acceptor

1. Introduction

Organic electronics offer numerous advantages over their inorganic counterparts, including a lower cost, greater flexibility, lighter weight, lower toxicity, and a greater functionality. Among organic electronic devices, organic solar cells (OSCs) are considered to be next-generation energy sources with the aforementioned advantages. Power conversion efficiencies (PCEs) greater than 16% have recently been reported as a result of the development of materials (e.g., fused-ring-based, small-molecule acceptors) and the optimization of device fabrication methods [1–3]. In 2020, more than 18% efficiency was reported by using a donor–acceptor (D-A) copolymer donor (D18) and a low bandgap acceptor (Y6) [4]. The active layers of OSCs have generally been composed of a polymer donor (D) and a small-molecule (or polymer) acceptor (A). To overcome the organic semiconductors' disadvantage of a limited light absorption range (they absorb only a part of the solar spectrum), researchers have widely used ternary or tandem devices to increase light absorption, thereby improving solar cell performance [5–7]. Ternary devices are more widely used than tandem cells because ternary devices are easier to manufacture. A photoactive organic semiconductor that exhibits complementary absorption is additionally introduced into a binary active layer, resulting in a ternary device (i.e., a D:D:A or D:A:A device). The important issues to be considered in the fabrication

of ternary devices are (1) the selection of the third material to be introduced into a given binary D:A system and (2) systematical control of the blend ratios. The selection of a third material with complementary light absorption is important, and the optimum blend ratio to prevent additional phase separation needs to be determined [8–12]. Recently, different working mechanisms and models of ternary systems have been proposed to explain the improved device characteristics: the cascade energy-level structure and the alloy-like structure. The alloy-like donors or acceptors, which are formed when two components are well mixed, result in tuned open-circuit voltage (V_{OC}) values that vary according to the blend ratios [13–16] and often offer a robust and stable morphology [17,18]. By contrast, the cascade energy-level alignment can provide a cascade driving force for electron (or hole) transfer, which enhances charge transfer and the short-circuit current density (J_{SC}) [19,20].

In our previous work, we reported three diketopyrrolopyrrole (DPP)-based small-molecule isomers for use as acceptors for poly(3-hexylthiophene) (P3HT)-based OSCs [21]. They were designed to have the same molecular backbone but differ in the position of the cyanide substituents (ortho, meta, or para), which greatly affects the molecules' packing behavior. In particular, the para-substituted molecule, *p*-DPP-PhCN, exhibited strong molecular aggregation, as confirmed by UV-vis absorption measurements, and we have reported how this different packing behavior affects the device performance of P3HT-based binary solar cells. Herein, we applied the *p*- and *o*-DPP-PhCN isomers in a ternary system to determine whether the different packing behaviors of the third component affect the device performance and the working mechanism of the ternary cells.

2. Materials and Methods

2.1. Physical Measurements

The UV-vis spectra were obtained using a Shimadzu UV/vis spectrometer. The DPP-PhCN and P3HT films used in the UV-vis measurements were prepared by spin coating from a chloroform (CF) solution or by drop-casing from an *o*-dichlorobenzene (*o*-DCB) solution. The electrochemical properties were studied by cyclic voltammetry (CV) with a BAS 100B electrochemical analyzer. A non-aqueous reference electrode (0.1 M Ag/Ag$^+$ acetonitrile solution), a platinum working electrode, and a platinum wire as a counter electrode were used as a three-electrode system. The redox potential of the materials was measured in acetonitrile with 0.1 M (n-C$_4$H$_9$)$_4$N-PF$_6$ at a scan rate of 100 mV s^{-1}. The films were prepared by dip coating the solution onto the platinum working electrode, and the measurements were calibrated using the ferrocenium/ferrocene (Fc) redox value of -4.8 eV as an external reference. The highest occupied molecular orbital (HOMO) and lowest unoccupied molecular orbital (LUMO) energy levels were estimated according to the empirical relationship $E_{HOMO} = -(E_{onset,ox} - E_{1/2,Fc} + 4.8)$ eV and $E_{LUMO} = -(E_{onset,red} - E_{1/2,Fc} + 4.8)$ eV, where $E_{onset,ox}$ and $E_{onset,red}$ are the onset potentials of oxidation and reduction, respectively, assuming that the energy level of Fc is 4.8 eV below the vacuum level [22–24].

2.2. Fabrication of OSC Devices

In the present work, the devices with the configuration ITO/PEDOT:PSS/active layer/LiF/Al were fabricated (where ITO is indium tin oxide and PEDOT:PSS is poly(3,4-ethylenedioxythiophene) polystyrene sulfonate (Clevios P VP AI 4083)). The ITO glass was cleaned with a sequential ultrasonic treatment in detergent, deionized water, acetone, and isopropyl alcohol for 15 min each and subsequently dried in an oven for 5 h. The ITO-coated glass substrates were pre-treated in a UV-ozone oven for 15 min. A layer of PEDOT:PSS (~30 nm) was spin-coated on top of the ITO-coated glass substrates at 4000 rpm and annealed at 100 °C for 10 min to remove residuary water in the PEDOT:PSS layer. The active layers were spin-cast at 3000 rpm from a D/A/A solution in CF and *o*-DCB with a total solids concentration of 15 and 40 mg mL^{-1}, respectively, followed by thermal annealing at 120 and 150 °C, respectively. The average thickness of the active layers using CF (~100 nm) and *o*-DCB (~200 nm) were measured with an Alpha-Step IQ

surface profiler. A LiF (~0.5 nm) and Al (~100 nm) layer were deposited via thermal evaporation on the active layer under a vacuum of ~10^{-6} Torr. The effective area of all devices was measured to be 9 mm^2. The current density vs. voltage (*J-V*) curves of the devices were measured using a computer-controlled Keithley 236 source measure unit. The characterization of un-encapsulated solar cells was carried out in air under AM 1.5G illumination (100 mW cm^{-2}) using a xenon lamp-based solar simulator. The simulator irradiance was characterized using a calibrated spectrometer, and the illumination intensity was set using an NREL-certified silicon diode with an integrated KG1 optical filter. The external quantum efficiency (EQE) was measured using a reflective microscope objective to focus the light output from a 100 W halogen lamp outfitted with a monochromator and optical chopper (PV Measurements, Inc., Point Roberts, WA, USA). The photocurrent was measured using a lock-in amplifier, and the absolute photon flux was determined using a calibrated silicon photodiode.

3. Results and Discussion

3.1. Materials and Physical Properties

Two DPP-based small molecules, *o*- and *p*-DPP-PhCNs, were selected as the third component to be incorporated into the P3HT:phenyl-C$_{61}$-butyric acid methyl ester (PCBM) system, resulting in P3HT:DPP-PhCN:PCBM ternary films. In our previous report, two DPP-PhCNs were synthesized using Pd-catalyzed Suzuki coupling reactions [21], in which the two small molecules had the same molecular backbone but differed in the position of the cyanide groups at the phenyl ends. The chemical structures of all the materials used in the active layer of the OSCs are shown in Figure 1.
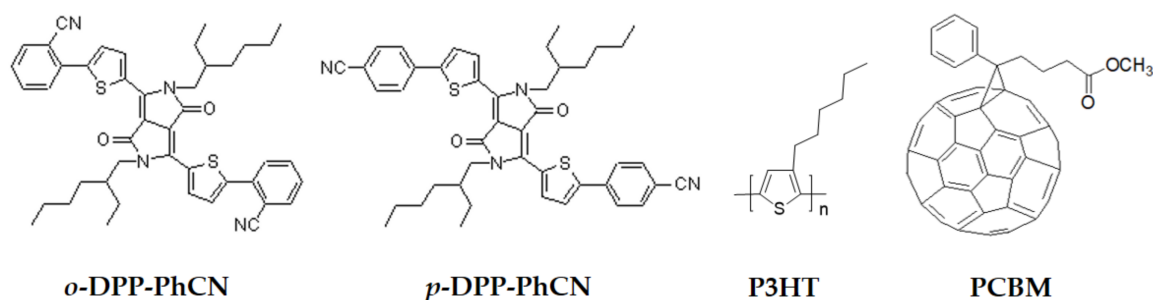
Figure 1. The chemical structures of the *o*- and *p*-diketopyrrolopyrrole (DPP)-PhCNs together with poly(3-hexylthiophene) (P3HT) and phenyl-C$_{61}$-butyric acid methyl ester (PCBM).

Figure 2a shows the normalized UV-vis absorption spectra of films of the two DPP-PhCNs and P3HT prepared from CF solutions. Although the two DPP-PhCNs had the same molecular backbone, their packing behaviors in the film state appeared to differ according to the position of the CN groups. The para-substitution resulted in more red-shifted absorption and in stronger molecular aggregation compared with the ortho-substitution. In the spectrum of the *p*-DPP-PhCN film, the absorption maximum (λ_{max}) of the low-energy band, which is assigned as the 0-0 transition, appeared at 670 nm, indicating a more effective π–π stacking between molecular backbones [25–28]. The optical bandgaps (E_gs) were obtained from the absorption onset (λ_{onset}) on the long-wavelength side ($E_g = 1240/\lambda_{onset}$). The *p*-DPP-PhCN exhibited a lower E_g (1.75 eV) compared with that of the *o*-DPP-PhCN (1.80 eV), consistent with the relatively stronger molecular packing of the *p*-DPP-PhCN molecules. The energy diagrams of the materials used in OSC fabrication are shown in Figure 2c. The HOMO level of the donor (P3HT) and the LUMO levels of the acceptors (DPP-PhCNs and PCBM) were measured by CV, and the LUMO of the donor and HOMO of the acceptors were calculated from the E_g values. The HOMO energy levels of the two DPP-PhCNs were found to be similar; however, for the LUMO energy levels, the para-substitution resulted in an energy level slightly lower than that of the ortho-substitution. The incorporation of DPP-PhCNs resulted in a cascade

energy-level alignment from P3HT, via DPP-PhCN, to PCBM in the P3HT:DPP-PhCN:PCBM ternary system.
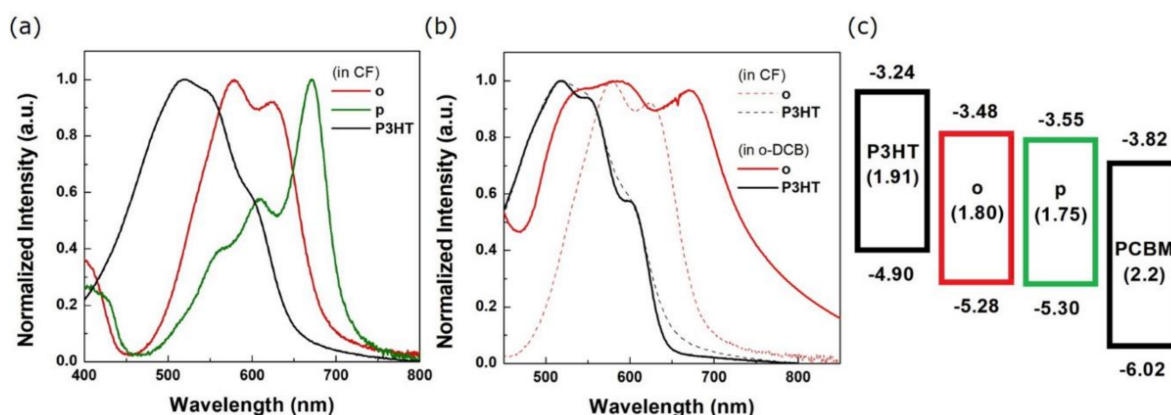
Figure 2. (**a**) Normalized UV absorption spectra of (**a**) the *o*-DPP-PhCN (o), *p*-DPP-PhCN (p), and P3HT films prepared from a chloroform (CF) solution and (**b**) the *o*-DPP-PhCN (o) and P3HT films prepared from CF and *o*- dichlorobenzene (DCB); (**c**) energy diagram of the materials used in organic solar cell (OSC) fabrication.

3.2. Device Performances

First, the two P3HT:DPP-PhCN devices were fabricated to evaluate the device performance of the binary devices with the configuration ITO/PEDOT:PSS/active layer/LiF/Al. Table 1 summarizes the photovoltaic performance of the binary cells measured in air under AM 1.5G illumination (100 mW cm^{-2}). The D:A blend ratio was adjusted to 1:1, as optimized in our previous report [21], and the same D:A ratio (1:1) was also used in the fabrication of the ternary cells used in the present work. CF and *o*-DCB were used as processing solvents. Both binary devices that were prepared using CF exhibited similar PCEs of ~0.46%. Compared with the V_{OC} of P3HT:*p*-DPP-PhCN (0.56 V), that of the P3HT:*o*-DPP-PhCN was greater (0.94 V), which can be explained by the relatively high-lying LUMO energy level of *o*-DPP-PhCN (-3.48 eV, Figure 2c) than that of *p*-DPP-PhCN (-3.55 eV). The V_{OC} of the P3HT:*p*-DPP-PhCN film appeared to be even lower than expected from the LUMO level of *p*-DPP-PhCN. The strong molecular aggregation of *p*-DPP-PhCN, as confirmed from UV-vis measurements, might better stabilize its LUMO level.

Table 1. Photovoltaic performances of the P3HT:DPP-PhCN binary cells.

Active Layer	Solvent	V_{OC} [V]	J_{SC} [mA cm^{-2}]	FF [%]	PCE [%]
P3HT:*o*-DPP-PhCN	CF [1]	1.09	1.19	35	0.46
	o-DCB	0.83	2.15	49	0.87
P3HT:*p*-DPP-PhCN	CF [1]	0.56	1.64	50	0.47

[1] Data taken from reference [21].

The P3HT:*p*-DPP-PhCN film prepared from *o*-DCB solution showed no photovoltaic characteristics because a uniform film morphology could not be obtained as a consequence of the poor solubility of *p*-DPP-PhCN in *o*-DCB. By contrast, the PCE of the P3HT:*o*-DPP-PhCN increased to 0.87% (Table 1) when high-boiling-point *o*-DCB was used as a processing solvent. The increase in efficiency mainly arose from the increase in the J_{SC} from 1.18 (CF) to 2.15 mA cm^{-2} (*o*-DCB). As depicted in Figure 2b, the absorption spectrum of the *o*-DPP-PhCN film prepared from *o*-DCB was much more red-shifted and broadened than that of the *o*-DPP-PhCN film prepared from CF, reflecting the increased molecular aggregation in the film prepared from *o*-DCB. This phenomenon is consistent with the increased J_{SC} value of the device prepared from *o*-DCB. The slight decrease in the V_{OC} of the device with the P3HT:*o*-DPP-PhCN film prepared from *o*-DCB originated from the enhanced molecular packing behavior of *o*-DPP-PhCN, which might result in a slight stabilization of its LUMO energy level.

Figure 3 shows the EQE responses of the binary solar cells (P3HT:DPP-PhCN), together with the UV-vis spectra of the neat films of each donor and acceptor used in the devices. In Figure 3a, the EQE response of the P3HT:*o*-DPP-PhCN device increased when the film prepared from *o*-DCB was used, matching its higher J_{SC} value. The EQE profiles matched the UV-vis absorption profiles well. When compared with the device with an *o*-DPP-PhCN film prepared from CF, the device with an *o*-DPP-PhCN film prepared from *o*-DCB showed an additional EQE peak in the longer-wavelength region at 690 nm, corresponding to the red-shifted λ_{max} peak of the *o*-DCB-processed *o*-DPP-PhCN film at 670 nm. In Figure 3b, the EQE maximum peak of the P3HT:*p*-DPP-PhCN device also corresponded to the λ_{max} peak of the *p*-DPP-PhCN film (670 nm).
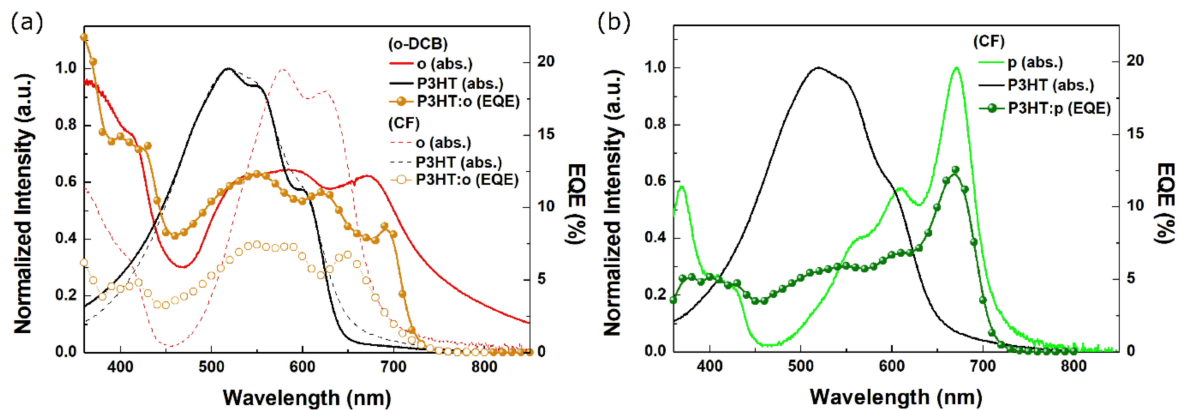
Figure 3. External quantum efficiency (EQE) responses of the binary solar cells fabricated with (**a**) P3HT:*o*-DPP-PhCN (o) and (**b**) P3HT:*p*-DPP-PhCN (p) films; the UV-vis spectra of the neat films of each donor and acceptor used in the devices are included for comparison.

The two DPP-PhCNs were then introduced into the active layer of P3HT:PCBM devices to fabricate ternary device cells. On the basis of the results of the binary devices, the ternary devices based on *o*-DPP-PhCN and *p*-DPP-PhCN were prepared from *o*-DCB and CF, respectively, and various blend ratios were investigated to optimize the performance of the devices. As control devices, P3HT:PCBM binary devices were also fabricated using both *o*-DCB and CF as processing solvents; these devices exhibited PCEs of 2.98% and 2.07%, respectively. The D:A blend ratio was adjusted to 1:1. The ternary P3HT:DPP-PhCN:PCBM film consisted of one donor (P3HT) and two acceptors (DPP-PhCN and PCBM), resulting in a D:A:A active layer. The total D:A ratio was maintained at 1:1. The ratio of the DPP-PhCN acceptor in the two-acceptor films was therefore varied; however, the total acceptor amount (i.e., DPP-PhCN + PCBM) was adjusted to be equal to the amount of the P3HT donor. The photovoltaic characteristics of the devices are summarized in Tables 2 and 3.

Table 2. Photovoltaic performances of the P3HT:*o*-DPP-PhCN:PCBM devices fabricated with films prepared using *o*-DCB as a solvent with various blend ratios.

Active Layer (D:A:A)	V_{OC} [V]	J_{SC} [mA cm^{-2}]	FF [%]	PCE [%]
4.0:0.0:4.0	0.60	8.03	62	2.98
4.0:0.4:3.6	0.61	7.94	61	2.95
4.0:0.8:3.2	0.63	7.70	59	2.86
4.0:1.2:2.8	0.64	7.20	59	2.72
4.0:1.6:2.4	0.65	7.42	55	2.67
4.0:2.0:2.0	0.67	6.31	45	1.92
4.0:4.0:0.0	0.83	2.15	49	0.87

Table 3. Photovoltaic performances the P3HT:*p*-DPP-PhCN:PCBM devices fabricated with films prepared using CF as a solvent with various blend ratios.

Active Layer (D:A:A)	V_{OC} [V]	J_{SC} [mA cm^{-2}]	FF [%]	PCE [%]
4.0:0.0:4.0	0.64	7.03	46	2.07
4.0:0.5:3.5	0.65	7.22	47	2.21
4.0:1.0:3.0	0.66	7.30	51	2.48
4.0:1.5:2.5	0.66	7.52	47	2.35
4.0:2.0:2.0	0.67	7.55	48	2.42
4.0:4.0:0.0	0.56	1.64	50	0.47

Figure 4 shows the *J-V* and EQE curves of the ternary devices based on P3HT:DPP-PhCN:PCBM in various blend ratios. In the ternary devices based on *o*-DPP-PhCN, as the ratio of *o*-DPP-PhCN increased, the device efficiency gradually decreased, mainly because of the decrease in the J_{SC} values (Figure 4a and Table 2). As the amount of *o*-DPP-PhCN increased, the EQE edge at the long-wavelength region, which included the contribution of light absorption by *o*-DPP-PhCN, was slightly red-shifted and broadened; however, the contribution of the light absorption of P3HT (~500 nm) to the EQE simultaneously decreased more significantly (Figure 4b). Consequently, the J_{SC} and PCE values gradually decreased with the increasing *o*-DPP-PhCN content. Notably, however, as the ratio of *o*-DPP-PhCN increased, the V_{OC} tended to gradually increase, as will be discussed later. By contrast, in the ternary device based on *p*-DPP-PhCN, the J_{SC} increased with the increasing ratio of *p*-DPP-PhCN (Figure 4c and Table 3). The best PCE of 2.48% was obtained at the blend ratio of 4:1:3 (P3HT:*p*-DPP-PhCN:PCBM). The increase in the J_{SC} can be explained by the pronounced shoulder peaks (670 nm) of the EQE curves (Figure 4d), which match the maximum EQE peak of the binary P3HT:*p*-DPP-PhCN device. Similar to the trend observed in ternary cells based on *o*-DPP-PhCN (Figure 4b), the EQE responses at ~500 nm gradually decreased with the increasing *p*-DPP-PhCN ratio; however, the increase in the EQE shoulder in the longer-wavelength region was more significant, resulting in a higher J_{SC} (Figure 4d).

The dependency of various photovoltaic parameters—J_{SC}, V_{OC}, fill factor (FF), and PCE—on the weight ratios of the DPP-PhCNs in the ternary cells are plotted in Figure 5. Among the *o*-DPP-PhCN-based cells (Figure 5a), the P3HT:*o*-DPP-PhCN binary cell exhibited a higher V_{OC} (0.83 V) than the P3HT:PCBM cell (0.60 V). All ternary devices that were prepared using both acceptors (*p*-DPP-PhCN and PCBM) exhibited V_{OC} values intermediate between the values corresponding to the two binary cells. With the increasing *o*-DPP-PhCN ratio, the V_{OC} values gradually increased. In the case of the *p*-DPP-PhCN-based cells, the binary P3HT:*p*-DPP-PhCN cell exhibited a lower V_{OC} (0.56 V) than that of the P3HT:PCBM cell (0.64 V). However, the V_{OC} values of the resulting ternary cells were not decreased by the addition of *p*-DPP-PhCN into P3HT:PCBM. The V_{OC} values of the ternary cells were approximately the same as that of P3HT:PCBM cell (slightly greater but within the error range). The difference in the trend of the V_{OC} variation according to the blend ratios indicates that the working mechanism of these two ternary systems differs. A V_{OC} that can be tuned by varying the ratio of the donors (or acceptors) has been previously observed in ternary solar cells with the alloy-like structure, where the two donors (or two acceptors) are mixed and form alloy-like domains, resulting in HOMOs (or LUMOs) that change in proportion to the blend ratios [20]. In our *o*-DPP-PhCN-based ternary cells, as the ratio of *o*-DPP-PhCN was increased from 0.0 to 1.0, the V_{OC} values proportionally increased from 0.60 to 0.83 V. The addition of *o*-DPP-PhCN with a relatively high-lying LUMO level positively affected the V_{OC} of the ternary cells. However, the V_{OC} of the *p*-DPP-PhCN-based ternary devices did not substantially vary upon the addition of *p*-DPP-PhCN, whereas the J_{SC} values gradually increased. In this case, we can propose that a cascade energy-level alignment might exist among the three materials rather than the alloy-like structure [19]. The cascade energy-level alignment is known to be beneficial for a charge transfer. In addition, because the V_{OC} values of the ternary cells are similar to those of P3HT:PCBM, the charge transfer from P3HT to PCBM might occur more effectively

than the transfer from P3HT to *p*-DPP-PhCN. Notably, the EQE curves of the ternary P3HT:*p*-DPP-PhCN:PCBM cells show substantial shoulder peaks at 670 nm, corresponding to the absorption of *p*-DPP-PhCN. In this cascade structure, a photoinduced hole transfer ("channel II" charge generation) by the light absorption of the acceptor (here, *p*-DPP-PhCN) contributes to the photocurrent generation of the devices, along with electron transfer induced by the absorption of the P3HT donor. These effects result in broad EQE responses and high J_{SC} values in the ternary cells. Improvements in device efficiencies by the cascade energy-level structure have been reported to occur as a result of more charge transport channels and complementary absorption [9,10]. The alloy-like structure observed for the combination of the two acceptors *o*-DPP-PhCN and PCBM is not formed between *p*-DPP-PhCN and PCBM because of the strong tendency of *p*-DPP-PhCN molecules to aggregate with each other. When the two acceptors were introduced as the third component of the ternary device, even though they had similar molecular structures, the working mechanism in the devices was found to differ substantially, where the molecular aggregation behavior played an important role. Further structural characterization of the small molecules, such as solid-state NMR spectroscopy and grazing incidence wide angle scattering [29–32], could potentially be achieved to investigate the impact of the molecular structure and the topology and morphology of the films on the photovoltaic performance of binary solar cells.
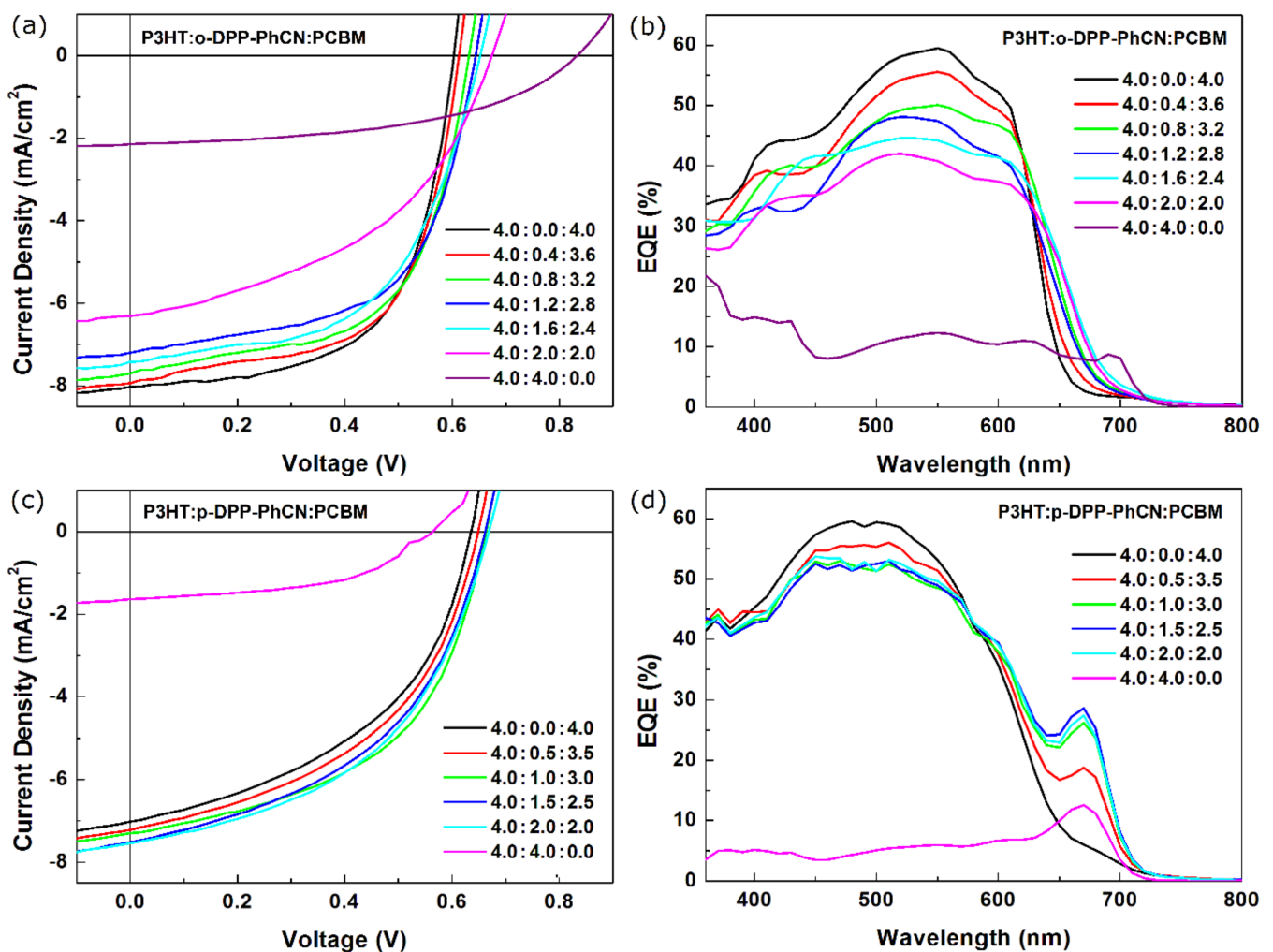
Figure 4. (**a**,**c**) Density vs. voltage (*J-V*) and (**b**,**d**) EQE curves of the ternary devices fabricated with various blend ratios of P3HT:*o*-DPP-PhCN:PCBM and P3HT:*p*-DPP-PhCN:PCBM.
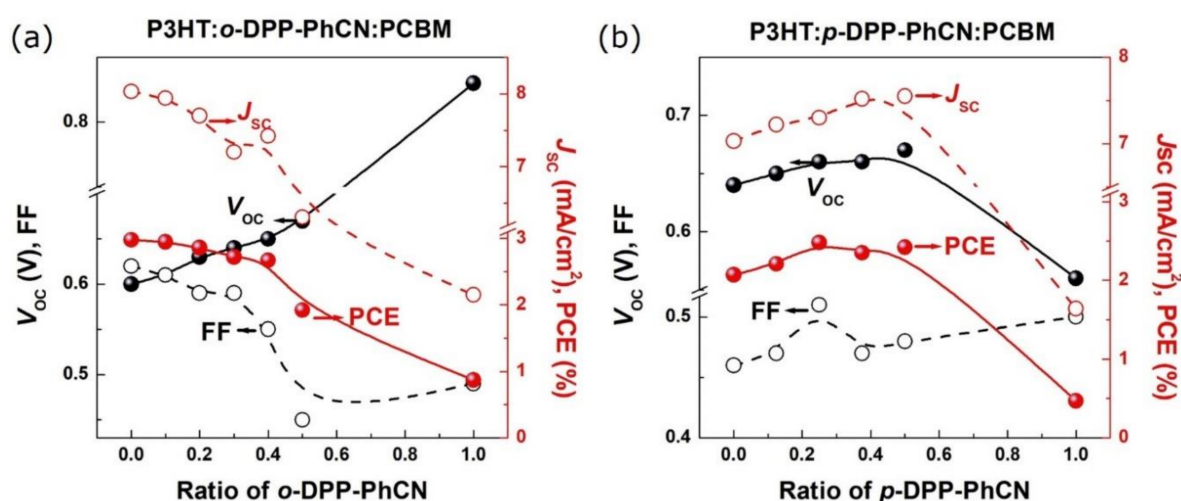
Figure 5. Dependence of the photovoltaic performance of ternary cells on the (**a**) *o*-DPP-PhCN and (**b**) *p*-DPP-PhCN blend ratios.

4. Conclusions

Herein, two DPP-based electron acceptors were introduced into the P3HT:PCBM system, resulting in ternary solar cells with the configuration ITO/PEDOT:PSS/P3HT:DPP-PhCN:PCBM/LiF/Al, and the device performance and the working mechanism were investigated according to the materials used and the blending ratios. Despite the similar molecular backbone of the two DPP-PhCNs, they exhibited very different packing behaviors according to the position of their CN substituents, which also greatly affected the working mechanism of the ternary devices in which the DPP-PhCNs were used as the third component. The working mechanisms for the o- and p-DPP-PhCN-based ternary cells were proposed to be the alloy-like structure and the cascade energy-level structure, respectively. In this study, the relationship between the crystallinity of the third component and the device characteristics was established to provide a detailed insight into the design and optimization of the third component to be introduced into a given binary system.

Data Availability Statement: Data is contained within the article.

Conflicts of Interest: The author declare no conflict of interest.

References

1. Lee, J.; Han, A.R.; Kim, J.; Kim, Y.; Oh, J.H.; Yang, C. Solution-Processable Ambipolar Diketopyrrolopyrrole–Selenophene Polymer with Unprecedentedly High Hole and Electron Mobilities. *J. Am. Chem. Soc.* **2012**, *134*, 20713–20721. [CrossRef] [PubMed]
2. Wu, L.; Xie, L.; Tian, H.; Peng, R.; Huang, J.; Fanady, B.; Song, W.; Tan, S.; Bi, W.; Ge, Z. Efficient ternary organic solar cells based on a twin spiro-type non-fullerene acceptor. *Sci. Bull.* **2019**, *64*, 1087–1094. [CrossRef]
3. Zhang, G.; Chen, X.K.; Xiao, J.; Chow, P.C.Y.; Ren, M.; Kupgan, G.; Jiao, X.; Chan, C.C.S.; Du, X.; Xia, R.; et al. Delocalization of exciton and electron wavefunction in non-fullerene acceptor molecules enables efficient organic solar cells. *Nat. Commun.* **2020**, *11*, 3943. [CrossRef] [PubMed]
4. Liu, Q.; Jiang, Y.; Jin, K.; Qin, J.; Xu, J.; Li, W.; Xiong, J.; Liu, J.; Xiao, Z.; Sun, K.; et al. 18% Efficiency organic solar cells. *Sci. Bull.* **2020**, *65*, 272–275. [CrossRef]
5. Rasi, D.D.C.; Janssen, R.A. Advances in Solution-Processed Multijunction Organic Solar Cells. *Adv. Mater.* **2019**, *31*, 1806499. [CrossRef]
6. Bi, P.; Hao, X. Versatile Ternary Approach for Novel Organic Solar Cells: A Review. *Sol. RRL* **2019**, *3*, 1800263. [CrossRef]
7. Lee, T.; Oh, S.; Rasool, S.; Song, C.E.; Kim, D.; Lee, S.K.; Shin, W.S.; Lim, E. Non-halogenated solvent-processed ternary-blend solar cells via alkyl-side-chain engineering of a non-fullerene acceptor and its application in large-area devices. *J. Mater. Chem. A* **2020**, *8*, 10318–10330. [CrossRef]
8. Fan, B.; Zeng, Z.; Zhong, W.; Ying, L.; Zhang, D.; Li, M.; Peng, F.; Li, N.; Huang, F.; Cao, Y. Optimizing Microstructure Morphology and Reducing Electronic Losses in 1 cm^2 Polymer Solar Cells to Achieve Efficiency over 15%. *ACS Energy Lett.* **2019**, *4*, 2466–2472. [CrossRef]

9.   Wang, J.; Ma, X.; Wang, J.; Ming, R.; An, Q.; Zhang, J.; Yang, C.; Zhang, F. Two Well-Compatible Acceptors with Efficient Energy Transfer Enable Ternary Organic Photovoltaics Exhibiting a 13.36% Efficiency. *Small* **2019**, *15*, 1902602. [CrossRef]

10.   Gao, H.-H.; Sun, Y.; Cai, Y.; Wan, X.; Meng, L.; Ke, X.; Li, S.; Zhang, Y.; Xia, R.; Zheng, N.; et al. Achieving Both Enhanced Voltage and Current through Fine-Tuning Molecular Backbone and Morphology Control in Organic Solar Cells. *Adv. Energy Mater.* **2019**, *9*, 1901024. [CrossRef]

11.   Liang, Z.; Tong, J.; Li, H.; Wang, Y.; Wang, N.; Li, J.; Yang, C.; Xia, Y. The comprehensive utilization of the synergistic effect of fullerene and non-fullerene acceptors to achieve highly efficient polymer solar cells. *J. Mater. Chem. A* **2019**, *7*, 15841–15850. [CrossRef]

12.   Gasparini, N.; Salleo, A.; McCulloch, I.; Baran, D. The role of the third component in ternary organic solar cells. *Nat. Rev. Mater.* **2019**, *4*, 229–242. [CrossRef]

13.   An, Q.; Wang, J.; Zhang, F. Ternary polymer solar cells with alloyed donor achieving 14.13% efficiency and 78.4% fill factor. *Nano Energy* **2019**, *60*, 768–774. [CrossRef]

14.   Chen, Y.; Ye, P.; Jia, X.; Gu, W.; Xu, X.; Wu, X.; Wu, J.; Liu, F.; Zhu, Z.-G.; Huang, H. Tuning Voc for high performance organic ternary solar cells with non-fullerene acceptor alloys. *J. Mater. Chem. A* **2017**, *5*, 19697–19702. [CrossRef]

15.   Zhang, M.; Ming, R.; Gao, W.; An, Q.; Ma, X.; Hu, Z.; Yang, C.; Zhang, F. Ternary polymer solar cells with alloyed non-fullerene acceptor exhibiting 12.99% efficiency and 76.03% fill factor. *Nano Energy* **2019**, *59*, 58–65. [CrossRef]

16.   An, Q.; Wang, J.; Gao, W.; Ma, X.; Hu, Z.; Gao, J.; Xu, C.; Hao, M.; Zhang, X.; Yang, C.; et al. Alloy-like ternary polymer solar cells with over 17.2% efficiency. *Sci. Bull.* **2020**, *65*, 538–545. [CrossRef]

17.   Zhao, Q.; Xiao, Z.; Qu, J.; Liu, L.; Richter, H.; Chen, W.; Han, L.; Wang, M.; Zheng, J.; Xie, Z.; et al. Elevated Stability and Efficiency of Solar Cells via Ordered Alloy Co-Acceptors. *ACS Energy Lett.* **2019**, *4*, 1106–1114. [CrossRef]

18.   Cheng, P.; Yan, C.; Wu, Y.; Wang, J.; Qin, M.; An, Q.; Cao, J.; Huo, L.; Zhang, F.; Ding, L.; et al. Alloy Acceptor: Superior Alternative to PCBM toward Efficient and Stable Organic Solar Cells. *Adv. Mater.* **2016**, *28*, 8021–8028. [CrossRef]

19.   Jiang, H.; Li, X.; Wang, J.; Qiao, S.; Zhang, Y.; Zheng, N.; Chen, W.; Li, Y.; Yang, R. Ternary Polymer Solar Cells with High Efficiency of 14.24% by Integrating Two Well-Complementary Nonfullerene Acceptors. *Adv. Funct. Mater.* **2019**, *29*, 1903596. [CrossRef]

20.   Wang, Z.; Zhu, X.; Zhang, J.; Lu, K.; Fang, J.; Zhang, Y.; Wang, Z.; Zhu, L.; Ma, W.; Shuai, Z.; et al. From Alloy-Like to Cascade Blended Structure: Designing High-Performance All-Small-Molecule Ternary Solar Cells. *J. Am. Chem. Soc.* **2018**, *140*, 1549–1556. [CrossRef] [PubMed]

21.   Kim, Y.; Song, C.E.; Ko, E.J.; Kim, D.; Moon, S.J.; Lim, E. DPP-based small molecule, non-fullerene acceptors for "channel II" charge generation in OPVs and their improved performance in ternary cells. *RSC Adv.* **2015**, *5*, 4811–4821. [CrossRef]

22.   Kwon, O.; Jo, J.; Walker, B.; Bazan, G.C.; Seo, J.H. Pendant group effects on the optical and electrical properties of carbazole-diketopyrrolopyrrole copolymers. *J. Mater. Chem. A* **2013**, *1*, 7118–7124. [CrossRef]

23.   Liu, D.; Kan, B.; Ke, X.; Zheng, N.; Xie, Z.; Lu, D.; Liu, Y. Extended Conjugation Length of Nonfullerene Acceptors with Improved Planarity via Noncovalent Interactions for High-Performance Organic Solar Cells. *Adv. Energy Mater.* **2018**, *8*, 1801618. [CrossRef]

24.   Daeneke, T.; Kwon, T.-H.; Holmes, A.B.; Duffy, N.W.; Bach, U.; Spiccia, L. High-efficiency dye-sensitized solar cells with ferrocene-based electrolytes. *Nat. Chem.* **2011**, *3*, 211–215. [CrossRef]

25.   Más-Montoya, M.; Janssen, R.A.J. The Effect of H- and J-Aggregation on the Photophysical and Photovoltaic Properties of Small Thiophene–Pyridine–DPP Molecules for Bulk-Heterojunction Solar Cells. *Adv. Funct. Mater.* **2017**, *27*, 1605779. [CrossRef]

26.   Lee, J.; Ko, H.; Song, E.; Kim, H.G.; Cho, K. Naphthodithiophene-Based Conjugated Polymer with Linear, Planar Backbone Conformation and Strong Intermolecular Packing for Efficient Organic Solar Cells. *ACS Appl. Mater. Interface* **2015**, *7*, 21159–21169. [CrossRef]

27.   Kim, J.S.; Fei, Z.; Wood, S.; James, D.T.; Sim, M.; Cho, K.; Heeney, M.J.; Kim, J.-S. Germanium- and Silicon-Substituted Donor–Acceptor Type Copolymers: Effect of the Bridging Heteroatom on Molecular Packing and Photovoltaic Device Performance. *Adv. Energy Mater.* **2014**, *4*, 1400527. [CrossRef]

28.   Bin, H.; Gao, L.; Zhang, Z.-G.; Yang, Y.; Zhang, Y.; Zhang, C.; Chen, S.; Xue, L.; Yang, C.; Xiao, M.; et al. 11.4% Efficiency non-fullerene polymer solar cells with trialkylsilyl substituted 2D-conjugated polymer as donor. *Nat. Commun.* **2016**, *7*, 13651. [CrossRef]

29.   Seifrid, M.; Reddy, G.N.M.; Chmelka, B.F.; Bazan, G.C. Insight into the structures and dynamics of organic semiconductors through solid-state NMR spectroscopy. *Nat. Rev. Mater.* **2020**, *5*, 910–930. [CrossRef]

30.   Seifrid, M.T.; Reddy, G.N.M.; Zhou, C.; Chmelka, B.F.; Bazan, G.C. Direct Observation of the Relationship between Molecular Topology and Bulk Morphology for a π-Conjugated Material. *J. Am. Chem. Soc.* **2019**, *141*, 5078–5082. [CrossRef]

31.   Karki, A.; Vollbrecht, J.; Dixon, A.L.; Schopp, N.; Schrock, M.; Reddy, G.N.M.; Nguyen, T.Q. Understanding the High Performance of over 15% Efficiency in Single-Junction Bulk Heterojunction Organic Solar Cells. *Adv. Mater.* **2019**, *31*, 1903868. [CrossRef] [PubMed]

32.   Karki, A.; Vollbrecht, J.; Gillett, A.J.; Xiao, S.S.; Yang, Y.; Peng, Z.; Schopp, N.; Dixon, A.L.; Yoon, S.; Schrock, M.; et al. The role of bulk and interfacial morphology in charge generation, recombination, and extraction in non-fullerene acceptor organic solar cells. *Energy Environ. Sci.* **2020**, *13*, 3679–3692. [CrossRef]